Progress In Electromagnetics Research M, Vol. 44, 1–12, 2015

Fixed-Image-Method-Based Transient Electromagnetic Model of Grounding System in Horizontally Stratified Multilayer Medium

Dino Lovrić* and Slavko Vujević

Abstract—In this paper, a frequency-domain-based transient electromagnetic model of grounding system in horizontally stratified multilayer medium is presented. The basis of the model is an improved version of the time-harmonic electromagnetic model of grounding system. Using the originally developed continuous numerical Fourier transform algorithm, the results obtained by the time-harmonic model are synthesized into a complete time domain solution. The presented model features very high accuracy and fast execution speed and is validated through several numerical examples.

1. INTRODUCTION

Grounding system analysis is generally considered to be a complex scientific and engineering field of study. This complexity stems from the fact that most approximations and simplifications used in other scientific fields are often unusable in grounding system analysis. For example, grounding system conductors can be long and short, but can neither be approximated by an infinite conductor nor by an infinitesimally small conductor. The conductors themselves can either be bare conductors or insulated cables with several layers of insulation. Furthermore, the ground in which these conductors are situated is highly heterogeneous in most cases. In most cases the ground is approximated by several horizontal layers [1–3] and, in some cases, even vertical [4] or spherical layers [5] all characterized by highly diverse soil parameters. Naturally since the grounding system conductors are buried in a lossy heterogeneous medium both longitudinal current which flows through the conductor and leakage current which flows into the surrounding medium must be taken into account. Last but not least, the current dissipated through the grounding system into the surrounding medium can be a time-harmonic current (50–60 Hz) for example during single pole short circuits or transient current which occurs for example during lightning strikes [6, 7]. In case of the transient current energization, all frequencies are present in the electromagnetic model, so researchers must choose whether to conduct the desired computations directly in the time domain [8] or indirectly in the frequency domain [9]. Both approaches have their advantages and disadvantages. The frequency-domain approach is generally considered to be faster and well suited to handle complex grounding systems, but cannot easily include nonlinear effects such as soil ionization [10]. In addition, the transformation procedure in frequency-domain-based models is problematic especially when using Fast Fourier Transform (FFT) [11, 12]. As can be seen from this brief summary of problems, the complexity of grounding system analysis is considerable but this complexity can be reduced if the result accuracy is sacrificed. Naturally, the goal would be to develop a well rounded electromagnetic model of the grounding system which will be as highly accurate as possible in the shortest execution time possible.

This paper will present a novel frequency-domain-based transient electromagnetic model of grounding system in horizontally stratified multilayer medium. This transient model introduces

Received 24 July 2015, Accepted 8 September 2015, Scheduled 1 October 2015

* Corresponding author: Dino Lovrić (dlovric@fesb.hr).

The authors are with the Faculty of Electrical Engineering, Mechanical Engineering and Naval Architecture, University of Split, Ruđera Boškovića 32, HR-21000 Split, Croatia.

improvements to previously published time-harmonic model of the grounding system [3, 13, 14] and features a novel algorithm for transformation purposes between the time and frequency domain and vice versa. These algorithms for continuous numerical Fourier transform (CNFT) [15] and inverse continuous numerical Fourier transform (ICNFT) [16] are robust, accurate and versatile which is clearly demonstrated in the aforementioned papers.

The developed transient electromagnetic model computes the quantities of interest on a set of frequencies using the time-harmonic electromagnetic model and then utilizes the originally developed CNFT/ICNFT algorithm [15, 16] to combine these results into a time domain solution. First, the transient current dissipated through the grounding system into the surrounding medium is transformed from the time domain into the frequency domain using CNFT. The developed algorithm can transform either a mathematical function or an actual measured lightning function [15]. Using CNFT, a continuous function of the transient current in the frequency domain is obtained using a combination of numerical and analytical integration of the Fourier integral. This consequently enables completely independent time domain and frequency domain sampling which is not feasible when using for example Fast Fourier Transform (FFT) algorithm [11, 12]. In the second step, electromagnetic quantities of interest for an arbitrary frequency set can be computed using the improved time-harmonic electromagnetic model. The procedure for selecting these frequencies is generalized and utilizes a combination of nonuniform and uniform sampling [16]. Finally in the third step, algorithm for ICNFT transforms the transient solution function from the frequency domain into the time domain using a combination of numerical and analytical integration.

In the time-harmonic electromagnetic model published in [3, 13, 14] and improved in this paper, conductors of the grounding system are subdivided into straight segments which satisfy the thin-wire approximation. Longitudinal current of the conductor segment is in the improved model approximated using a linear approximation instead of a constant as used in [3, 13, 14]. Complete electromagnetic coupling between segments is taken into account. Computation of Sommerfeld integrals is circumvented using an effective approximation of the attenuation and phase shift effects which significantly contributes to the execution speed of the model [3, 13, 14]. Segments of the grounding system can be situated in any layer of the horizontally stratified multilayer medium which includes the air layer and an arbitrary number of ground layers. Influence of layers is taken into account by using the highly accurate and numerically stable fixed image method developed in previous work [17]. This time-harmonic electromagnetic model of a grounding system can be used to compute all electromagnetic quantities of interest for a chosen frequency in observation point(s) situated in any layer of the medium: scalar electric potential, magnetic vector potential, magnetic flux density and electric field intensity.

The accuracy of the presented transient electromagnetic model will be verified by comparing it with published results obtained both by calculation and by measurement.

2. CONTINUOUS NUMERICAL FOURIER TRANSFORM OF TRANSIENT CURRENT DISSIPATED THROUGH THE GROUNDING SYSTEM INTO THE SURROUNDING GROUND

When performing frequency-domain-based transient computations a reliable procedure is required for transformation of an arbitrary transient source current from the time domain into the frequency domain. In other words, in the first computation step the transient current $i(t)$ that is dissipated through the grounding grid into the surrounding medium needs to be transformed to the frequency domain. In paper [15], a reliable and highly accurate numerical algorithm was developed for continuous transformation of an arbitrary transient current waveform from the time domain into the frequency domain. The developed CNFT algorithm is based on arbitrary discretization of the transient current function in the time domain (adaptive recursive sampling is used) and linearization of the lightning current function over a time segment. This enables analytical transformation of the transient current into the frequency domain, thus resulting in a continuous expression in the frequency domain [15]:

$$\bar{I}_{CNFT}(\omega) = \sum_{k=1}^{NEL_t} \frac{(i_{k+1} - i_k) \cdot \bar{A}_k + (t_{k+1} \cdot i_k - t_k \cdot i_{k+1}) \cdot \bar{B}_k}{t_{k+1} - t_k} \tag{1}$$

where for $\omega \neq 0$:

$$\bar{A}_k = \frac{e^{-j\cdot\omega\cdot t_{k+1}} - e^{-j\cdot\omega\cdot t_k}}{\omega^2} + j\cdot\frac{t_{k+1}\cdot e^{-j\cdot\omega\cdot t_{k+1}} - t_k\cdot e^{-j\cdot\omega\cdot t_k}}{\omega} \tag{2}$$

$$\bar{B}_k = j\cdot\frac{e^{-j\cdot\omega\cdot t_{k+1}} - e^{-j\cdot\omega\cdot t_k}}{\omega} \tag{3}$$

while for $\omega = 0$:

$$\bar{A}_k = \frac{t_{k+1}^2 - t_k^2}{2} \tag{4}$$

$$\bar{B}_k = t_{k+1} - t_k \tag{5}$$

In Equation (1), NEL_t represents the total number of finite elements in the time domain over which the transient current is linearized, t_k the starting time of the k-th finite element, t_{k+1} the ending time of the k-th finite element, $i_k = i(t_k)$ the value of the transient current in the k-th global nod, $i_{k+1} = i(t_{k+1})$ the value of the transient current in the global node k+1, t the time, $\omega = 2\cdot\pi\cdot f$ the circular frequency, and f the frequency.

For more details about the sampling procedure used in the CNFT algorithm refer to [15]. The developed CNFT algorithm was extensively tested and its accuracy and versatility were validated on several numerical examples [15].

3. TIME-HARMONIC ANALYSIS OF GROUNDING SYSTEM IN HORIZONTALLY STRATIFIED MULTILAYER MEDIUM

In this section, the basic theoretical background of the improved time-harmonic model of the grounding system in horizontally stratified multilayer medium is presented. The presented formulas are valid for one frequency value so consequently this time-harmonic model needs to be invoked as many times as there are sampled frequency values. The total number and values of the sampled frequencies are determined by the algorithm used in the ICNFT algorithm presented in paper [16].

In the presented time-harmonic model of the grounding system all computations of interest are performed including computation of potentials and computation of electromagnetic fields in any number of observation points. The presented model can deal with grounding systems comprised of arbitrarily positioned bare cylindrical conductors. In the time-harmonic model these conductors are divided into segments in such a way that thin-wire approximation is satisfied. The time-harmonic model of the grounding system is based on finite element technique and the entire set of grounding grid conductor segments forms one finite element. For the purpose of formation of the complete local system of equations all conductor segments are initially disconnected (Fig. 1). Fig. 1 also depicts the selected indexation of local nodes. As can be seen, the beginning nodes of segments are denoted from 1 to Ns whereas the ending nodes are denoted from Ns+1 to $2\cdot Ns$.

In the time-harmonic model, grounding grid conductor segments are situated in horizontally stratified multilayer medium, and they can be positioned in any layer of the medium. The first layer of the medium is the air layer while other layers represent the multilayer earth model. The total number of earth layers can be completely arbitrary. An arbitrary i-th layer is described by its thickness and complex wave propagation constant $\bar{\gamma}_i = j\cdot\omega\cdot\mu_0\cdot(\sigma_i + j\cdot\omega\cdot\varepsilon_0\cdot\varepsilon_{ri})$ where μ_0 is the medium permeability of the vacuum, σ_i is electrical conductivity of the i-th layer, ε_0 is the permittivity of vacuum and ε_{ri} is the relative permittivity of the i-th earth layer. The effect of medium heterogeneity is taken into account by using the fixed image method originally developed in [17] and used in [3, 13, 14]. Basically, this fixed image method utilized the imaging method to take into account various earth layer configurations. For segments parallel to earth surface the heterogeneity of the medium is taken into account by using three exact images of the segment and 30 fixed images of the segment [3]. In the case of nonparallel segments this heterogeneity is taken into account by using three exact images and 30 fixed images of five point current sources positioned along the conductor axis [13]. For more details refer to [17].

Since the conductor segments are situated in lossy medium, the current of the segments flows both through the conductor and into the surrounding medium (Fig. 2).

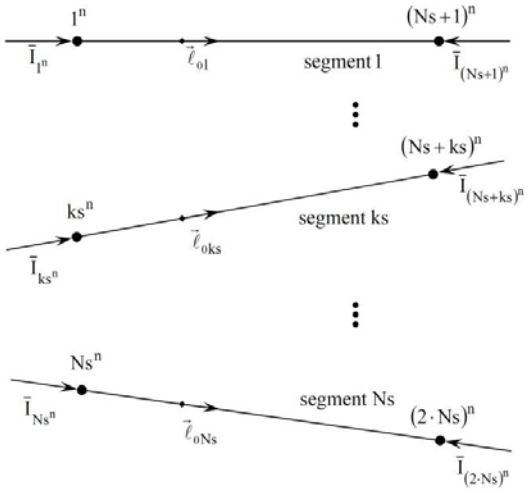

Figure 1. Disconnected grounding system conductor segments.

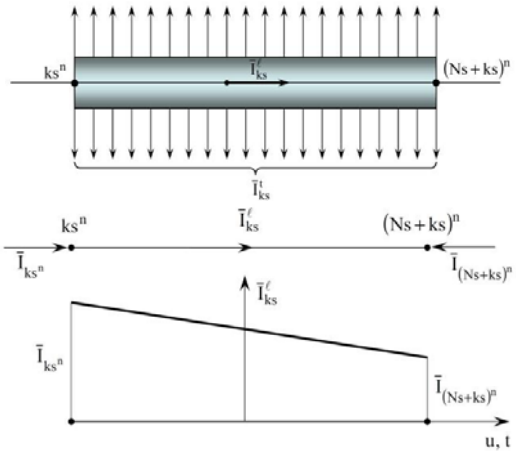

Figure 2. Approximation of the grounding system conductor segment current.

In the improved time-harmonic electromagnetic model of the grounding system, the current of the *ks*-th conductor segment which flows along the segment axis (longitudinal current) is approximated linearly along the segment using the following expression:

$$\bar{I}^{\ell}_{ks}(u) = N_{ks^n} \cdot \bar{I}_{ks^n} + N_{(Ns+ks)^n} \cdot \bar{I}_{(Ns+ks)^n} \tag{6}$$

$$N_{ks^n}(u) = \frac{1-u}{2} \tag{7}$$

$$N_{(Ns+ks)^n}(u) = -\frac{1+u}{2} \tag{8}$$

where $\bar{I}_{ks^n}$ is the nodal current of the beginning node of the *ks*-th segment and $\bar{I}_{(ks+Ns)^n}$ the nodal current of the ending node of the *ks*-th segment (Fig. 2). This consequently implies that the transversal current of the conductor segment that leaks into the surrounding medium is constant along the segment length:

$$\bar{I}^{t}_{ks}(u) = \bar{I}_{ks^n} + \bar{I}_{(Ns+ks)^n} \tag{9}$$

In the finite element technique the complete local system of equations first needs to be formed. Using Galerkin-Bubnov method a system of linear equations for longitudinal and transversal segment currents is initially formed which can then easily be transformed to an equivalent complete local system of linear equations for nodal currents:

$$\begin{bmatrix} [\bar{Z}^t] & [\bar{Z}^t] \\ [\bar{Z}^{b\ell}] & [\bar{Z}^{e\ell}] \end{bmatrix} \cdot \{{}^n\bar{I}\} = \begin{bmatrix} \frac{1}{2}\cdot[E] & \frac{1}{2}\cdot[E] \\ [E] & [E] \end{bmatrix} \cdot \{{}^n\bar{\Phi}\} \tag{10}$$

where $[\bar{Z}^t]$ is a symmetrical transversal segment impedance matrix, $[\bar{Z}^{b\ell}]$ a nonsymmetrical matrix of longitudinal impedances between segments and beginning nodes of segments, $[\bar{Z}^{e\ell}]$ a nonsymmetrical matrix of longitudinal impedances between segments and ending nodes of segments, $[E]$ the unit matrix, $\{{}^n\bar{I}\}$ a vector representing local nodal currents, and $\{{}^n\bar{\Phi}\}$ a vector representing local nodal potentials. Elements of the symmetrical transversal segment impedance matrix $[\bar{Z}^t]$ are computed analytically and have been derived in detail in [3] and [13, 14] whereas the nonsymmetric matrices $[\bar{Z}^{e\ell}]$ and $[\bar{Z}^{e\ell}]$ represent improvements to the previously developed model and are computed numerically using an improved Gaussian quadrature.

Longitudinal impedance between the *ks*-th segment and the beginning of the same segment is

computed using the following expression:

$$\bar{Z}^{b\ell}_{ks,ks^n} = \frac{\ell_{ks}}{2} \cdot \bar{Z}^1_{ks} + \bar{f}_{ks,ks} \cdot \frac{j \cdot \omega \cdot \mu_0}{4 \cdot \pi} \cdot \int\limits_{-\frac{\ell_{ks}}{2}}^{\frac{\ell_{ks}}{2}} \int\limits_{-\frac{\ell_{ks}}{2}}^{\frac{\ell_{ks}}{2}} \frac{N_{ks^n}(t)}{\sqrt{(t-u)^2 + v^2}} dt \cdot du \tag{11}$$

where ℓ_{ks} is the length of the ks-th conductor segment, $\bar{Z}^1_{ks}$ the per-unit-length internal impedance of the ks-th segment and $\bar{f}_{ks,ks}$ the attenuation-phase shift factor which approximately takes into account phase shift and attenuation effects between the ks-th segment and the beginning node of the ks-th segment [3, 13, 14]. The exact expression for this attenuation — phase shift factor can be found in [3, 13, 14] along with an in-depth validation of using this factor instead of solving numerically very ill behaved Sommerfeld integrals.

Longitudinal impedance between the is-th segment and the beginning node of the ks-th segment is computed using the following expression:

$$\bar{Z}^{b\ell}_{is,ks^n} = \left(\vec{\ell}_{0is} \cdot \vec{\ell}_{0ks}\right) \cdot \bar{f}_{is,ks} \cdot \frac{j \cdot \omega \cdot \mu_0}{4 \cdot \pi} \cdot \int\limits_{-\frac{\ell_{is}}{2}}^{\frac{\ell_{is}}{2}} \int\limits_{-\frac{\ell_{ks}}{2}}^{\frac{\ell_{ks}}{2}} \frac{N_{ks^n}(t)}{\sqrt{(t-u)^2 + v^2}} dt \cdot du \tag{12}$$

where $\vec{\ell}_{0ks}$ is the unit vector of the ks-th conductor segment and $\bar{f}_{is,ks}$ the attenuation-phase shift factor which approximately takes into account phase shift and attenuation effects between the is-th segment and the beginning node of the ks-th segment. The elements of the nonsymmetric matrix $[\bar{Z}^{e\ell}]$ are calculated using the following expressions similar as before:

$$\bar{Z}^{e\ell}_{ks,ks^n} = \frac{\ell_{ks}}{2} \cdot \bar{Z}^1_{ks} + \bar{f}_{ks,ks} \cdot \frac{j \cdot \omega \cdot \mu_0}{4 \cdot \pi} \cdot \int\limits_{-\frac{\ell_{ks}}{2}}^{\frac{\ell_{ks}}{2}} \int\limits_{-\frac{\ell_{ks}}{2}}^{\frac{\ell_{ks}}{2}} \frac{N_{(Ns+ks)^n}(t)}{\sqrt{(t-u)^2 + v^2}} dt \cdot du \tag{13}$$

$$\bar{Z}^{e\ell}_{is,ks^n} = \left(\vec{\ell}_{0is} \cdot \vec{\ell}_{0ks}\right) \cdot \bar{f}_{is,ks} \cdot \frac{j \cdot \omega \cdot \mu_0}{4 \cdot \pi} \cdot \int\limits_{-\frac{\ell_{is}}{2}}^{\frac{\ell_{is}}{2}} \int\limits_{-\frac{\ell_{ks}}{2}}^{\frac{\ell_{ks}}{2}} \frac{N_{(Ns+ks)^n}(t)}{\sqrt{(t-u)^2 + v^2}} dt \cdot du \tag{14}$$

The complete local system of equations can be obtained from (10) by rearranging the expression to:

$$\left[\bar{Y}\right] \cdot \left\{{}^n\bar{\Phi}\right\} = \left\{{}^n\bar{I}\right\} \tag{15}$$

where $[\bar{Y}]$ represents the nodal admittance matrix of the local system which can be derived from Eq. (10).

By equalizing the elements of the nodal current vector with zero, the incomplete local system of equations is obtained and is ready for the assembly procedure:

$$\left[\bar{Y}\right] \cdot \left\{{}^n\bar{\Phi}\right\} = \{0\} \tag{16}$$

Using the assembly procedure the previously disconnected segments become connected in global nodes:

$$\left[\bar{Y}_g\right] \cdot \left\{\bar{\Phi}_g\right\} = \{0\} \tag{17}$$

where $[\bar{Y}_g]$ is the admittance matrix of global nodes and $\{\bar{\Phi}_g\}$ the unknown vector of global nodal potentials. Finally, the complete global system of equations is obtained by imposing the known boundary conditions, i.e., the injected currents into any of the global nodes:

$$\left[\bar{Y}_g\right] \cdot \left\{\bar{\Phi}_g\right\} = \left\{\bar{I}_g\right\} \tag{18}$$

The injected currents are obtained using the CNFT algorithm described in the previous section. Finally, when the unknown global potentials are computed then it is easy to calculate local node potentials and consequently local nodal currents which are needed for computation of longitudinal and

transversal segment currents. These segment currents are required for computation of scalar electric potential, vector magnetic potential and electromagnetic fields.

Algorithm for computation of scalar electric potential in an arbitrary observation point has been published in [13] whereas the algorithms for computation of vector magnetic potential and electromagnetic fields are fairly straightforward and are not presented here due manuscript page limitation. Nevertheless, this computed quantity (potential and/or electromagnetic field) represents the solution function and needs to be computed as many times as there are sampled frequency values. Then this solution function needs to be transformed back to the time domain. This is accomplished using the inverse continuous numerical Fourier transform (ICNFT) developed in paper [16] and concisely presented in the following section.

4. INVERSE CONTINUOUS NUMERICAL FOURIER TRANSFORM OF THE SOLUTION FUNCTION COMPUTED IN AN ARBITRARY OBSERVATION POINT

The solution function is transformed back to the time domain using ICNFT algorithm developed in paper [16]. Let the solution function be denoted by $\bar{F}(\omega)$. ICNFT algorithm utilizes nonuniform sampling in the frequency domain to determine the optimal number and value of the sampled frequencies which is described in detail in paper [16]. For each of these sampled frequencies time-harmonic electromagnetic model from the previous section is invoked to calculate the solution function in one or more observation points. The developed ICNFT algorithm is based on arbitrary discretization of the transient solution function in the frequency domain and linearization of the solution function over a frequency segment. This enables analytical transformation of the solution function into the time domain, thus resulting in a continuous expression in the time domain [16]:

$$f_{ICNFT}(t) = \frac{1}{\pi} \cdot \sum_{k=1}^{NEL_\omega} \mathrm{Re}\left[\frac{\left(\bar{F}_{k+1} - \bar{F}_k\right) \cdot \bar{C}_k + \left(\omega_{k+1} \cdot \bar{F}_k - \omega_k \cdot \bar{F}_{k+1}\right) \cdot \bar{D}_k}{\omega_{k+1} - \omega_k} \right] \tag{19}$$

where for $t \neq 0$:

$$\bar{C}_k = \frac{e^{j \cdot \omega_{k+1} \cdot t} - e^{j \cdot \omega_k \cdot t}}{t^2} + j \cdot \frac{\omega_k \cdot e^{j \cdot \omega_k \cdot t} - \omega_{k+1} \cdot e^{j \cdot \omega_{k+1} \cdot t}}{t} \tag{20}$$

$$\bar{D}_k = j \cdot \frac{e^{j \cdot \omega_k \cdot t} - e^{j \cdot \omega_{k+1} \cdot t}}{t} \tag{21}$$

while for $t = 0$:

$$\bar{C}_k = 0; \quad \bar{D}_k = 0 \tag{22}$$

In Equation (19), NEL_ω represents the total number of finite elements in the frequency domain over which the transient solution function is linearized, ω_k the starting circular frequency of the k-th finite element, ω_{k+1} the ending circular frequency of the k-th finite element, $\bar{F}_k = \bar{F}(\omega_k)$ the value of the solution function in the k-th global node, and $\bar{F}_{k+1} = \bar{F}(\omega_{k+1})$ the value of the solution function in the global node k+1.

The developed ICNFT algorithm was extensively tested and its accuracy and versatility were validated on several numerical examples [16]. The main advantage of the presented CNFT/ICNFT algorithms is the independence of sampling points in the time and frequency domains thus enabling the user much faster and adaptable computation than in the case when FFT/IFFT is used. This even enables the user to perform nonlinear computations in the frequency-domain-based model iteratively. This, for example, means that soil ionization can be effectively taken into account even though this is a frequency domain based model.

5. NUMERICAL EXAMPLES

In the following three numerical examples results obtained using the presented transient electromagnetic model will be compared to measured data [18] and to results computed using full electromagnetic models from literature [19, 20]. In the first numerical example comparison is made with results computed using a full electromagnetic model and results obtained by measurement in two-layer earth on a simple

grounding system [18, 19]. In the second numerical example comparison is made with results obtained using a full electromagnetic model in homogeneous earth on a complex grounding system [20]. In this example the disadvantages of using FFT/IFFT algorithm in transient grounding grid analysis are clearly depicted. The third numerical example will demonstrate the advantages of using the proposed transient electromagnetic model. Two connected grounding system buried in 4-layer earth are observed and scalar electric potential is computed in 23511 observation points located on the earth surface.

5.1. Comparison with Measured Data and a Full Electromagnetic Model for a Simple Grounding System in Two-Layer Ground

In this example, results obtained by the proposed model will be compared to measured data from [18] and results obtained by a full electromagnetic model which numerically solves Sommerfeld integrals [19]. The observed grounding system is depicted in Fig. 3 and formed by copper conductors ($50\,\text{mm}^2$ cross section). The ground is approximated by two layers. The resistivity of the first layer is $50\,\Omega\text{m}$, and relative permittivity of the first layer is 10, whereas the resistivity of the second layer is $26\,\Omega\text{m}$ with the same permittivity as the first layer. In the conducted experiment from [18], impulse current is injected into the grounding system in point A, and scalar electric potential is measured and computed in that same point. Actual measured injected current along with its double-exponential approximation used for simulation is depicted in Fig. 4. Double-exponential approximation was used because approximation is also used in the full electromagnetic model [19]. Parameters of the double-exponential function obtained using the least squares method [21] are: $I_0 = 10.2\,\text{A}$, $\eta = 0.84421$, $\alpha = 10917.74\,\text{s}^{-1}$ and $\beta = 284259.97\,\text{s}^{-1}$.

In the developed numerical model, the grounding system is subdivided into 24 equal segments of 2.5 m length. Scalar electric potential in point A is computed in 294 sampled frequencies with maximum circular frequency being $\omega_{\max} = 184.2025 \cdot 10^6\,\text{rad/s}$. After this, ICNFT was used to transform the frequency domain results to the time domain. Fig. 5 depicts three curves of scalar electric potential in observation point A: (a) measured data [18], (b) results obtained using full electromagnetic model [19] and (c) results obtained using the proposed electromagnetic model. As can be seen excellent agreement of results was found.

The proposed transient electromagnetic model can work with actual measured current as input data unlike most models available in literature. When computing the scalar electric potential in point A with the measured current as the source current, scalar electric potential in point A was computed in 357 sampled frequencies with maximum circular frequency being $\omega_{\max} = 3.9831 \cdot 10^9\,\text{rad/s}$. Then again ICNFT was used to transform the results into the time domain. The obtained results are depicted in Fig. 6 and as can be seen good agreement with measured data has been found.

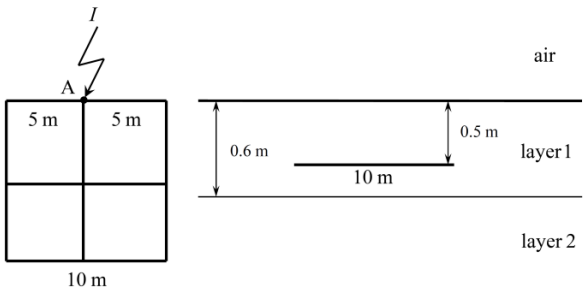

Figure 3. Layout of the observed grounding system buried in two-layer ground.

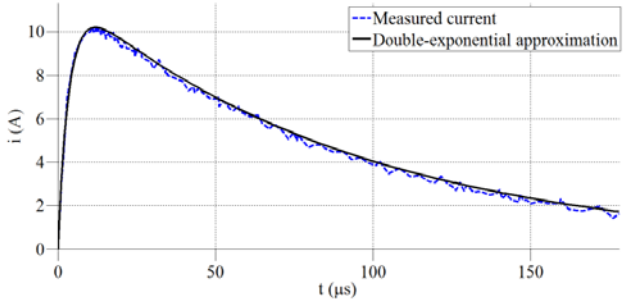

Figure 4. Measured current injected into node A and its double-exponential approximation.

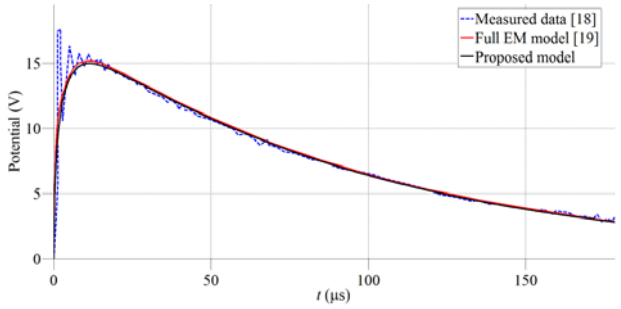

Figure 5. Comparison of scalar electric potential in point A computed using the proposed model with measured data and results computed using the full electromagnetic model [18].

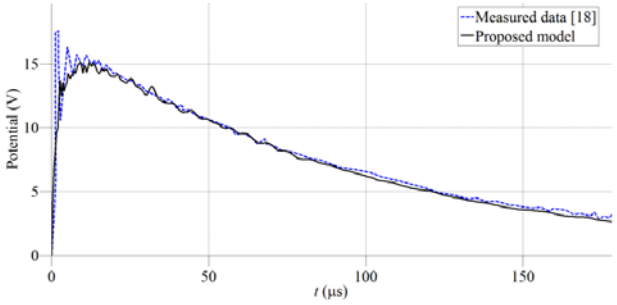

Figure 6. Comparison of measured scalar electric potential in point A and results obtained using the proposed model when the injected current is the actual measured current.

5.2. Comparison with a Full Electromagnetic Model for a Complex Grounding System in Homogeneous Ground

This example features a complex grounding system situated in homogeneous ground (Fig. 7). The resistivity of ground is 100 Ωm, and its relative permittivity is 36. Lightning current is injected into the central point of the grounding system A, and the scalar electric potential is computed in points A, B and C using the proposed model and a full electromagnetic model [20] which numerically solves Sommerfeld integrals and utilizes the FFT/IFFT algorithm. Grounding system is buried at a depth of 0.6 m parallel with the earth surface and is composed of copper conductors of 4.6 mm radius (Fig. 7).

Lightning current waveform 1/20 μs with a 1 kA peak value is injected in point A. Unfortunately, in paper [20] it is not stated, whose lightning current function is used to approximate this 1/20 μs waveform, so in this paper Heidler function was used. The following Heidler function parameters were obtained using the least squares method [22]: $I_0 = 1\,\text{kA}$, $\eta = 0.90294$, $\tau_1 = 0.3186\,\mu\text{s}$, $\tau_2 = 25.1575\,\mu\text{s}$ and $n = 2$. Scalar electric potential in observation points A, B and C is computed using the proposed model and compared to the full electromagnetic model [20].

In the developed numerical model, the grounding system is subdivided into 176 equal segments of 5 m length. Scalar electric potentials in points A, B and C are computed in 331 sampled frequencies with frequency being $\omega_{\text{max}} = 1.12021 \cdot 10^9$ rad/s. After this, ICNFT was used to transform the frequency domain results to the time domain. Figs. 8–10 depict comparisons of results for points A, B and C between the proposed model and the full electromagnetic model [20].

The disadvantages of using FFT/IFFT algorithm are evident from previous figures. When using FFT/IFFT algorithm in transient analysis, it is necessary to select the time window in such a way that

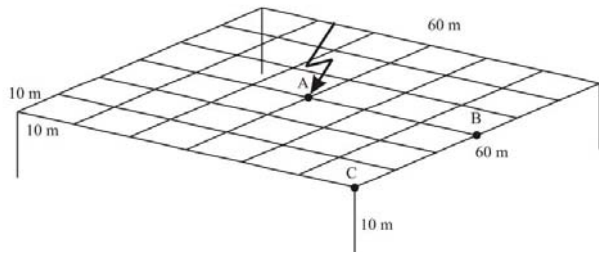

Figure 7. Observed grounding system in homogeneous ground.

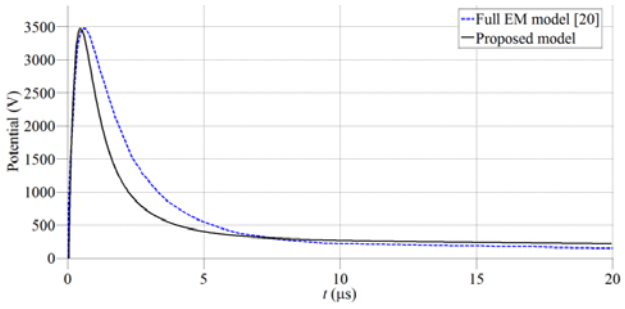

Figure 8. Comparison of scalar electric potentials computed using the proposed model and full electromagnetic model from [19] in point A.

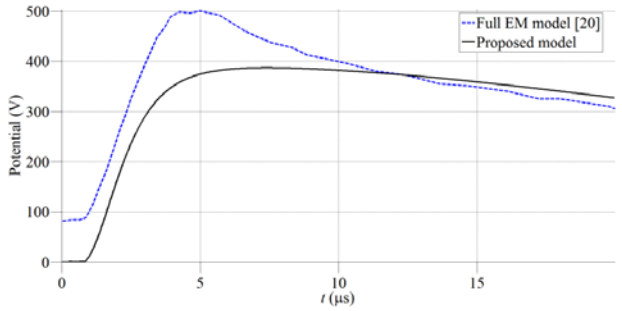

Figure 9. Comparison of scalar electric potentials computed using the proposed model and full electromagnetic model from [19] in point B.

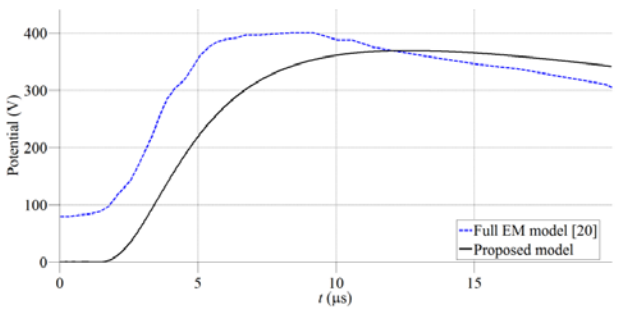

Figure 10. Comparison of scalar electric potentials computed using the proposed model and full electromagnetic model from [19] in point C.

both the source function and the solution function must become insignificant at that instant. Since in some cases computations are performed in several observation points, the optimal value of the time window is not identical for all points. This is evident from Figs. 9 and 10 where one can observe a DC component which is introduced in the results which makes them physically invalid since the results do not start from zero for $t = 0$. A detailed overview of disadvantages of FFT in transient analysis is presented in [12].

5.3. 3D Computation of Scalar Electric Potential for Two Simple Grounding Systems in 4-Layer Ground

In this numerical example, two simple grounding systems are observed. They are buried in 4-layer ground at a depth of 0.5 m (see Figs. 11–12) and connected by a 200 m long copper conductor. All grounding system conductors are copper conductor with a 4.6 mm radius. The characteristics of the ground layers are presented in Table 1.

Scalar electric potentials are computed in 23511 observation points that form an observational surface positioned at ground level, extending above the grounding grids. In other words, observational

Table 1. haracteristics of ground layers.

Index of Ground Layer	Resistivity (Ωm)	Relative Permittivity
1	1000	10
2	800	8
3	700	9
4	2000	10

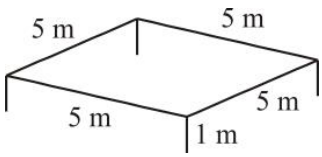

Figure 11. Observed grounding system.

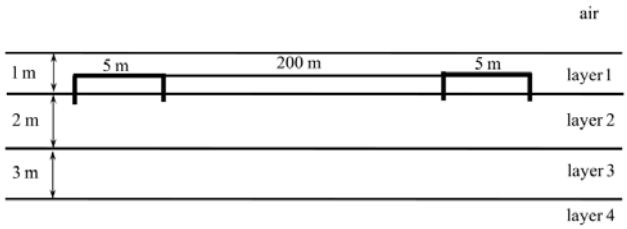

Figure 12. Two connected grounding systems in 4-layer ground.

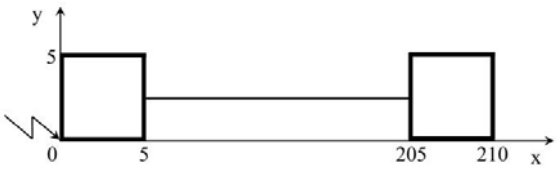

Figure 13. Layout of the grounding systems.

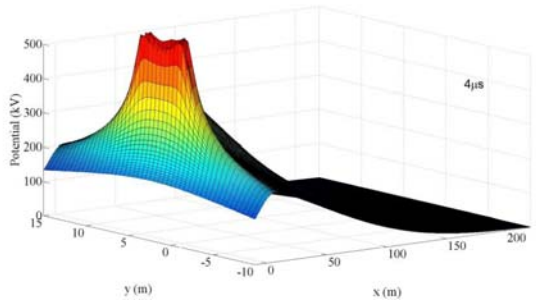

Figure 14. Scalar electric potential in 23511 observation points on the earth surface at $t = 4\,\mu s$.

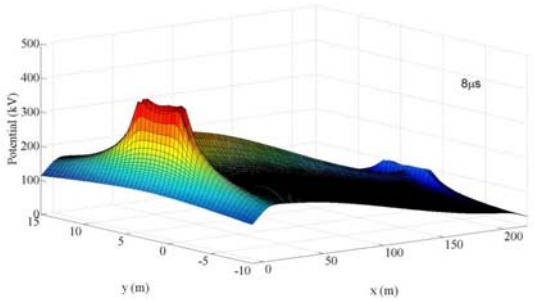

Figure 15. Scalar electric potential in 23511 observation points on the earth surface at $t = 8\,\mu s$.

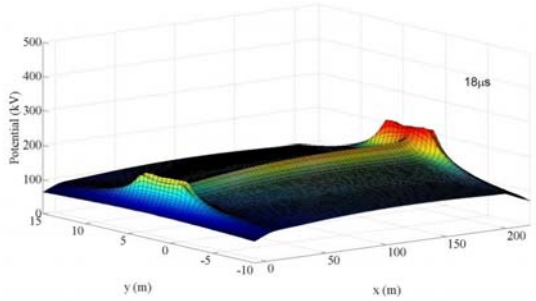

Figure 16. Scalar electric potential in 23511 observation points on the earth surface at $t = 18\,\mu s$.

surface is a rectangle positioned at earth level where $-10 \leq x \leq 210$ and $-10 \leq y \leq 15$ with field points spread 1 m apart. This example is near to impossible to perform when using FFT/IFFT because for every observation point different FFT parameters are required. In the proposed model when using CNFT/ICNFT algorithm this is unnecessary.

A lightning current modeled by Heidler function is injected into the corner of one grounding system (Fig. 13). Parameters of the Heidler employed in this example are: $I_0 = 28\,kA$, $\eta = 0.8231$, $\tau = 0.8231$, $\tau_1 = 1.8\,\mu s$, $\tau_2 = 30\,\mu s$ and $n = 2$.

In the transient electromagnetic model, each grounding grid is subdivided into 20 horizontal segments of 1 m length and 8 vertical segments of 0.5 m length while the connecting conductor is subdivided into 100 equal segments of 2 m length. This makes a total of 156 segments. Using the proposed algorithm scalar electric potential was computed at 23511 observation points at 281 sampled frequencies ($\omega_{max} = 97.639 \cdot 10^6$ rad/s). After this, ICNFT was used to transform the frequency domain results to the time domain. This means that for each observation point a time domain curve of the scalar electric potential exists. Figs. 14–16 depicts the time domain propagation of scalar potential in 23511 observation points.

6. CONCLUSION

In this paper, a transient electromagnetic model of grounding system in horizontally stratified multilayer medium is concisely presented. The model utilizes a novel transformation algorithm for continuous numerical Fourier transform which significantly improves the quality and accuracy of results. The basis of the transient electromagnetic model is an improved version of previously published time-harmonic electromagnetic model of grounding system. The resulting transient electromagnetic model features very high accuracy and execution speed. This combination of speed and accuracy is achieved mainly because of these three reasons: accurate approximation of attenuation and phase shift effects which circumvents the solving of Sommerfeld integrals, utilization of the fixed image method to account for an arbitrary number of soil layers and utilization of the continuous numerical Fourier transform

algorithm for transformation purposes between the time and frequency domain. In addition, although this transient electromagnetic model is a frequency domain based model, it can include nonlinear effects of soil ionization in computation procedure due to mutually independent sampling in the time and frequency domain in the presented transformation algorithm.

REFERENCES

1. Li, Z.-X., W. Chen, J. B. Fan, and J. Lu, "A novel mathematical modeling of grounding system buried in multilayer earth," *IEEE Transactions on Power Delivery*, Vol. 21, No. 3, 1267–1272, 2006.
2. Arnautovski-Toševa, V. and L. Grčev, "A comparison of exact and image model for HF analysis of horizontal grounding conductors in two-layer soil," *Proceedings of the 6th International Conference on Applied Electromagnetics*, 5–8, Niš, Serbia and Montenegro, 2003.
3. Sarajčev, P., S. Vujević, and D. Lovrić, "Time-harmonic current distribution on conductor grid in horizontally stratified multilayer medium," *Progress In Electromagnetics Research B*, Vol. 31, 67–87, 2011.
4. Colominas, I., et al., "Computer analysis of earthing systems in horizontally or vertically layered soils," *Electric Power Systems Research*, Vol. 59, No. 3, 149–156, 2001.
5. Ma, J., F. P. Dawalibi, and W. K. Daily, "Analysis of grounding systems in soils with hemispherical layering," *IEEE Transactions on Power Delivery*, Vol. 8, No. 4, 1773–1781, 1993.
6. Sarajčev, P. and S. Vujević, "A review of methods for grounding grid analysis," *Proceedings of the 17th International Conference on Software, Telecommunications & Computer Networks*, 42–49, Split-Hvar-Korčula, Croatia, 2009.
7. Sarajčev, P. and S. Vujević, "Grounding grid analysis: Historical background and classification of methods," *International Review of Electrical Engineering*, Vol. 4, No. 4, 670–683, 2009.
8. Liu, Y., M. Zitnik, and R. Thottappillil, "An improved transmission line model of grounding system," *IEEE Transactions on Electromagnetic Compatibility*, Vol. 43, No. 3, 348–355, 2001.
9. Grcev, L. and F. Dawalibi, "An electromagnetic model for transients in grounding systems," *IEEE Transactions on Power Delivery*, Vol. 5, No. 4, 1773–1781, 1990.
10. Mousa, M., "The soil ionization gradient associated with discharge of high currents into concentrated electrodes," *IEEE Transactions on Power Delivery*, Vol. 9, No. 3, 1669–1677, 1994.
11. Chu, E. and A. George, *Inside the FFT Black Box, Serial and Parallel Fast Fourier Transform Algorithms*, CRC Press, Boca Raton, 2000.
12. Lovrić, D., S. Vujević, and P. Sarajčev, "Accuracy of the Inverse Fast Fourier Transform in grounding grid transient analysis," *Proceedings of the 20th International Conference on Applied Electromagnetics and Communications*, (S10-3) 1–4, Dubrovnik, Croatia, 2010.
13. Vujević, S., P. Sarajčev, and D. Lovrić, "Time-harmonic analysis of grounding system in horizontally stratified multilayer medium," *Electric Power Systems Research*, Vol. 83, 28–34, 2011.
14. Sarajčev, P., S. Vujević, and D. Lovrić, "Computing the electromagnetic field of the system of arbitrarily positioned conductors in horizontally stratified multilayer medium," *International Journal of Numerical Modelling — Electronic Networks, Devices and Fields*, Vol. 28, No. 2, 121–137, 2015.
15. Vujević, S. and D. Lovrić, "On continuous numerical Fourier transform for transient analysis of lightning current related phenomena," *Electric Power Systems Research*, Vol. 119, 364–369, 2015.
16. Vujević, S. and D. Lovrić, "Inverse continuous numerical Fourier transform for transient analysis of electromagnetic phenomena," *IEEE Transactions on Electromagnetic Compatibility*, Published online, doi: 10.1109/TEMC.2015.2417654, 2015.
17. Vujević, S. and P. Sarajčev, "Potential distribution for a harmonic current point source in horizontally stratified multilayer medium," *The International Journal for Computation and Mathematics in Electrical and Electronic Engineering*, Vol. 27, 624–637, 2008.

18. Stojković, Z., M. S. Savić, J. M. Nahman, D. Salamon, and B. Bukorović, "Sensitivity analysis of experimentally determined grounding grid impulse characteristics," *IEEE Transactions on Power Delivery*, Vol. 13, No. 4, 1136–1142, 1998.
19. Arnautovski-Toševa, V. and L. Grčev, "Transient analysis of grounding grids in twolayer soil," *Proceedings of 7th International Conference on Applied Electromagnetics*, 360–370, Niš, Serbia and Montenegro, 2005.
20. Grcev, L. D., "Computer analysis of transient voltages in large grounding systems," *IEEE Transactions on Power Delivery*, Vol. 11, No. 2, 815–823, 1996.
21. Lovrić, D., S. Vujević, and T. Modrić, "Least-squares estimation of double-exponential function parameters," *Proceedings of the 11th International Conference on Applied Electromagnetics*, (O2-4) 1–4, Niš, Serbia, 2013.
22. Vujević, S., D. Lovrić, and I. Jurić-Grgić, "Least squares estimation of Heidler function parameters," *European Transactions on Electrical Power*, Vol. 21, No. 1, 505–521, 2011.